SLAC-PUB-11238
May 2005

Analysis of Positron Collection in the Linear Collider*

Yuri K. Batygin

Stanford Linear Accelerator Center, Stanford University, Stanford, CA 94309

Abstract

In the Linear Collider, the positron capture system includes a positron production target, an adiabatic matching device (AMD), and a linac to accelerate positrons up to the injection energy of the positron damping ring. Efficiency of the positron collector is defined by the number of positrons accepted into the damping ring. Analysis of the positron collection system is performed using a conventional scheme, where positrons are produced by a high-energy electron beam hitting the high-Z target. The collection system has been optimized to insure high positron capture into the 6-dimensional acceptance of the damping ring. Various parameters affecting the positron capture are analyzed.

Presented at 2005 Particle Accelerator Conference, May 16-20, 2005, Knoxville, TN, USA

*Work is supported by Department of Energy Contract No. DE-AC02-76SF00515

ANALYSIS OF POSITRON COLLECTION IN THE LINEAR COLLIDER*

Yuri K. Batygin, SLAC, Stanford, CA 94309, USA

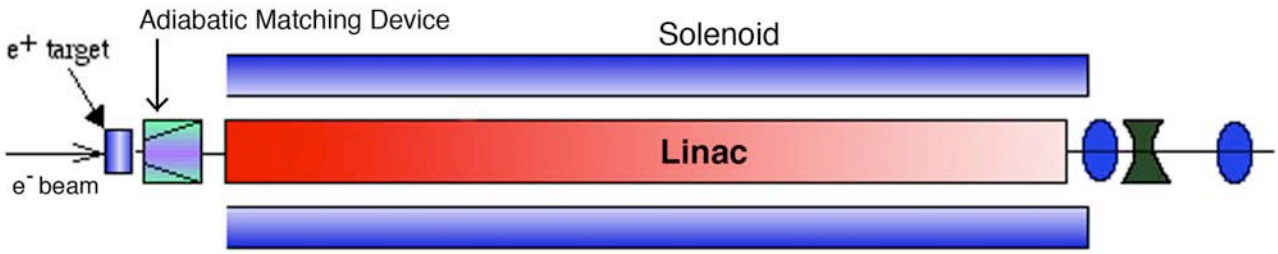

Fig. 1. Layout of positron injector.

Abstract

In the Linear Collider, the positron capture system includes a positron production target, an adiabatic matching device (AMD), and a linac to accelerate positrons up to the injection energy of the positron damping ring (see Fig. 1). Efficiency of the positron collector is defined by the number of positrons accepted into the damping ring. Analysis of the positron collection system is performed using a conventional scheme, where positrons are produced by a high-energy electron beam hitting the high-Z target. The collection system has been optimized to insure high positron capture into the 6-dimensional acceptance of the damping ring. Various parameters affecting the positron capture are analyzed.

POSITRON BEAM PARAMETERS AFTER THE TARGET

Parameters of conventional positron collector system are presented in Table 1. Fig.2 illustrates the process of positron production from a single 6 GeV electron hitting W-23Re 4.5 RL target. Shower develops close to the exit of the target and the resulting secondary particles have large divergence. Positron beam distribution generated by 6 GeV electron beam with transverse Gaussian distribution with $\sigma_x = \sigma_y$ =1.5 mm is presented in Fig. 3. The resulting positron beam has a narrow spot and large transverse momentum and energy spread.

Positron yield as a function of target length is presented in Fig. 4. Positron yield has a maximum Y_{max}=13.2 at the L= 5.5 RL. The same figure illustrates positron yield within specific normalized emittance. Partial positron yield has a maximum at L = 4…6 RL.

Two parameters are important to characterize the efficiency of positron collection. Positron yield, $Y=N_{e+}/N_{e-}$, is a ratio of the number of accepted positrons N_{e+}, to the number of incident electrons, N_{e-}. Positron capture, $C = N_{e+}/N_{e+,target}$ is a ratio of accepted positrons to number of positrons produced at the target, $N_{e+,taget}$.

*Work is supported by the Department of Energy Contract No DE-AC02-76SF00515

Table 1. Parameters of positron collector

Target	
Material	77W23Re
Length	4.5 RL
Electron Beam	
Energy	6 GeV
Transverse size, $\sigma_x = \sigma_y$	1.5…..2 mm
Longitudinal size, σ_t	1.5 …..5 ps
Adiabatic Matching Device	
Field at the target, B_{max}	6 Tesla
Field coefficient, g	0.6 cm^{-1}
Field Length	18 cm
Pre-Accelerator	
Wavelength	23 cm
Accelerating gradient	12 MeV/m
Focusing magnetic field	0.5 Tesla

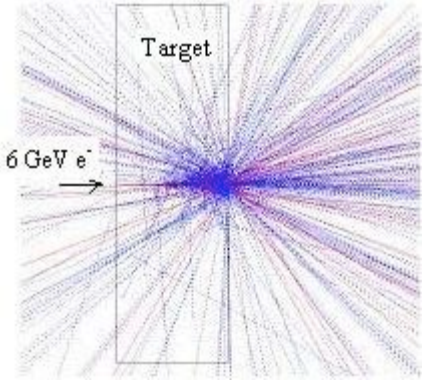

Fig. 2. GEANT3 simulation of pair production from a single 6 GeV electron: (blue) photons, (red) electrons and positrons.

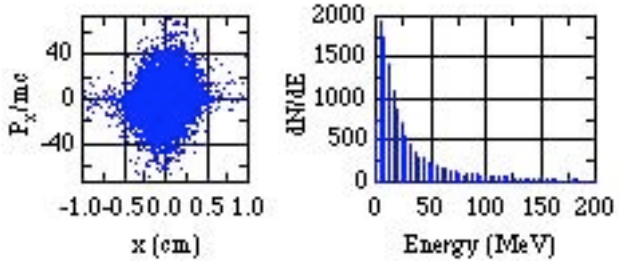

Fig. 3. Positron distribution after target.

PARTICLE DYNAMICS IN ADIABATIC MATCHING DEVICE

The positron beam extracted from the target has to be transformed into the beam with small transverse momentum spread and a larger spot to be matched with the focusing structure of a linac. Transformation is performed in an adiabatic matching device where the magnetic field slowly decreases from the large value at the target, B_{max} = 6 Tesla, to the nominal value of the focusing field in the linac, B_o = 0.5 Tesla, along z-direction (see Fig. 5). Field distribution along z-direction is described by [1]

$$B_z = \frac{B_{max}}{1 + gz}, \qquad (1)$$

where parameter g defines field profile.

Adiabatic variation of parameters is achieved when change of magnetic field per particle revolution is small with respect to the value of the field. It is well-known, that in adiabatic processes the adiabatic invariant is conserved:

$$I = \frac{1}{2\pi}\left[\int P_x dx + \int P_y dy\right] = \frac{e B_z \rho^2}{2}, \qquad (2)$$

where ρ is the radius of particle orbit, and I is the phase space area comprised by a single-particle trajectory. Particle with energy γ and longitudinal momentum $P_z = mc\beta_z\gamma$ performs one revolution in the magnetic field at the time $T = 2\pi m\gamma/(eB_z)$. During this time, the particle moves at the distance of $z_o = 2\pi P_z/(eB_z)$. The change of the magnetic field at that distance has to be small to fulfill the adiabatic condition, $(dB_z/dz)z_o << B_z$. Taking into account Eq. (1), it can be written as

$$\delta = \frac{2\pi P_z}{e}\left|\frac{d B_z/dz}{B_z^2}\right| = 2\pi \frac{P_z g}{eB_{max}} << 1. \qquad (3)$$

Fig. 5 illustrates single-particle trajectory in the AMD. The particle starts oscillation at a small deviation from the axis and reaches a large value of transverse momentum. After a few oscillations, the particle is matched with a low magnetic field of B = 0.5 Tesla with small momentum and larger deviation from the axis. Due to the adiabaticity of the process, initial and final phase space areas are equal to each other with good accuracy. If the number of turns per AMD decreases, which corresponds to an increase of parameter δ, the final phase space area becomes larger than the initial one (see Fig. 6). With a further increase of parameter δ, the final phase space area comprised by a single-particle trajectory might be smaller than one for low-energy positrons, because for very high-energy particles, the AMD is similar to a thin lens.

Fig. 7 illustrates particle distributions after AMD for two versions of the field profile. Field with g = 0.078 cm^{-1} corresponds to "long" adiabatic field profile. In this case,

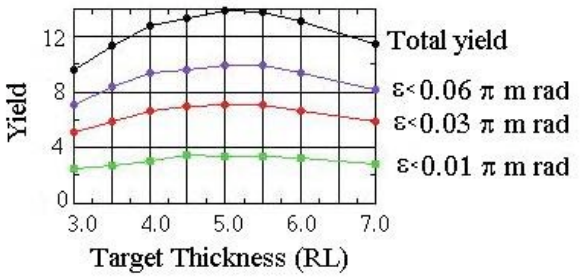

Fig. 4. Positron yield as a function of target thickness.

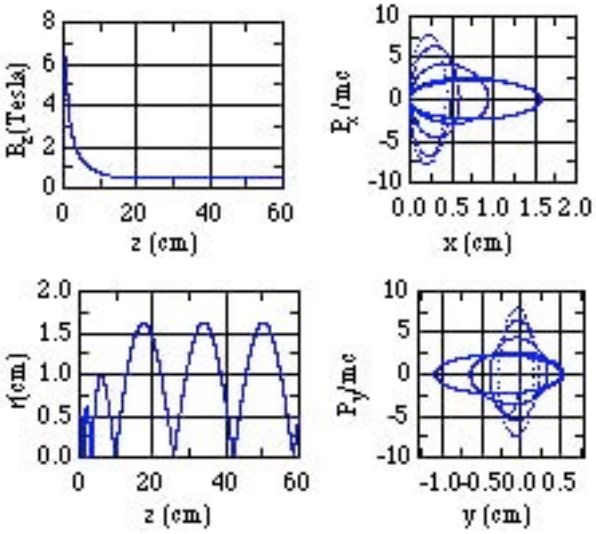

Fig. 5. Single particle trajectory in AMD.

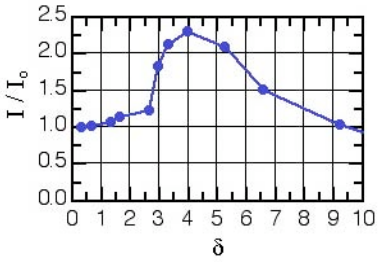

Fig 6. Adiabatic invariant as a function of parameter δ.

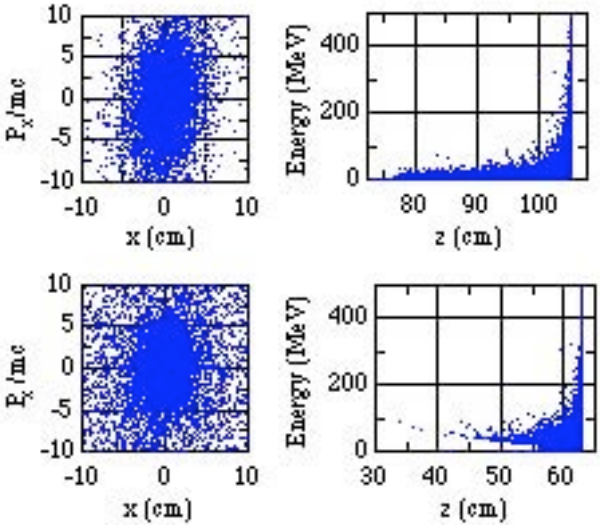

Fig. 7. Positron beam distribution after AMD; (up) g = 0.078 cm^{-1}, (bottom) g = 0.78 cm^{-1}.

transverse particle distribution conserves well, however, the bunch length after AMD is large. For a "short" adiabatic field profile with g = 0.78 cm^{-1} the final bunch is shorter, however the beam emittance growth is large. Fig.8 illustrates positron phase space density of the beam after AMD with different values of parameter g. Combination of two contradictionary factors (adiabatic conservation of transverse beam distribution and bunch lengthening) results in appearance of a maximum of positron capture at g = 0.6 cm^{-1} (see Fig. 9).

ACCELERATION OF POSITRONS

After the AMD, the positrons are accelerated up to the injection energy into the damping ring. Fig. 10 contains positron distribution at 5 GeV. While the transverse positron distribution is mostly conserved in the linear optics channel, the longitudinal distribution is curved in the RF field. It is convenient to analyze the particle acceleration using longitudinal mapping in RF field [2]:

$$\sin\varphi = \sin\varphi_o - \frac{2\pi\, mc^2}{e\, E\, \lambda}\left(\frac{\gamma_o}{\beta_w} - \sqrt{\gamma_o^2 - 1 - p_t^2}\right), \qquad (4)$$

$$\gamma = \gamma_o + \frac{eE}{mc^2} L \cos\varphi , \qquad (5)$$

where E is the accelerating gradient, λ is the wavelength, L is the accelerator length, γ_o is the initial energy, γ is the final energy, φ_o is the initial phase , φ is the final phase, $p_t^2 = (P_x^2 + P_y^2)/(mc)^2$ is the square of normalized transverse momentum, and β_w is the wave velocity.

Fig. 11 illustrates the positron capture as a function of the accelerating gradient. For large values of the gradient, the second term in Eq. (4) is negligible with respect to the first term and the positron capture is irrelevant to the value of E. If the value of the gradient drops, RF phase of each positron is changed according to Eq. (4) and the number of positrons within a specific energy spread becomes smaller. Similar dependence appears for positron capture as a function of wavelength. With an increase of wavelength, the RF bunch width becomes smaller, which results in an increase of positron capture.

Fig. 12 illustrates the positron yield as a function of phase space area occupied by the beam at the energy of 5 GeV. The positron yield can reach the values of Y=1.0….1.3 for particles accepted within edge phase space area of $\varepsilon_x = \varepsilon_y \le 0.03\ \pi$ m rad, and energy resolution of $\Delta E/E \le 1\ldots2\%$.

REFERENCES

[1] R.H.Helm, SLAC-4 (1962).

[2] M.James, R.Donahue, R.Miller and W.Nelson, NIM A307, p.p. 207-212 (1991).

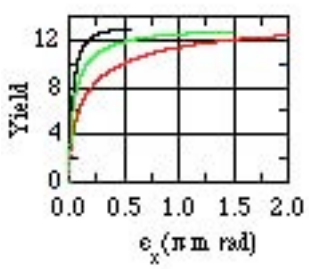

Fig. 8. Positron yield as a function of beam emittance: (black) after target, (green) after AMD with g = 0.078 cm^{-1} , (red) after AMD with g=0.78cm^{-1}.

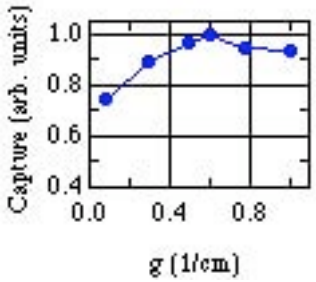

Fig. 9 . Positron capture as a function of parameter g.

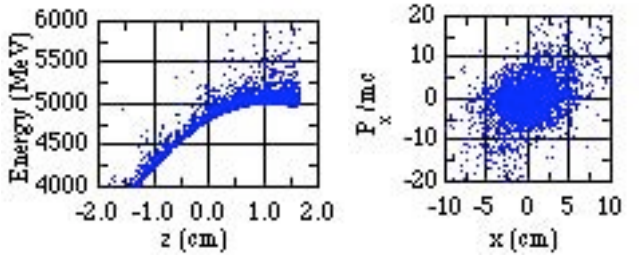

Fig. 10 . Positron beam distribution at 5 GeV.

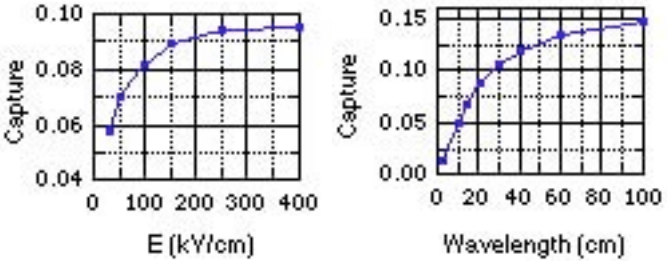

Fig. 11. Positron capture as a function of accelerating gradient and wavelength.

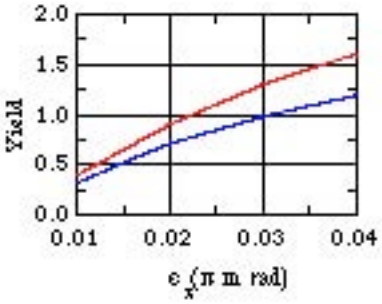

Fig. 12. Positron yield at 5 GeV as a function of beam emittance : (blue) $\Delta E/E < 1\%$, (red) $\Delta E/E < 2\%$.